

Dirac and Nodal Line Magnons in Three-Dimensional Antiferromagnets

Kangkang Li,^{1,2} Chenyuan Li,³ Jiangping Hu,^{1,4} Yuan Li,^{3,4,*} and Chen Fang^{1,†}

¹Beijing National Laboratory for Condensed Matter Physics, and Institute of Physics,
Chinese Academy of Sciences, Beijing 100190, China

²University of Chinese Academy of Sciences, Beijing 100049, China

³International Center for Quantum Materials, School of Physics, Peking University, Beijing 100871, China

⁴Collaborative Innovation Center of Quantum Matter, Beijing 100871, China

(Received 29 March 2017; revised manuscript received 7 October 2017; published 13 December 2017)

We study the topological properties of magnon excitations in three-dimensional antiferromagnets, where the ground state configuration is invariant under time reversal followed by space inversion (PT symmetry). We prove that Dirac points and nodal lines, the former being the limiting case of the latter, are the generic forms of symmetry-protected band crossings between magnon branches. As a concrete example, we study a Heisenberg spin model for a “spin-web” compound, Cu_3TeO_6 , and show the presence of the magnon Dirac points assuming a collinear magnetic structure. Upon turning on symmetry-allowed Dzyaloshinsky-Moriya interactions, which introduce a small noncollinearity in the ground state configuration, we find that the Dirac points expand into nodal lines with nontrivial Z_2 -topological charge, a new type of nodal line not predicted in any materials so far.

DOI: 10.1103/PhysRevLett.119.247202

Introduction.—The theoretical proposal [1,2] and experimental discovery [3–5] of Weyl semimetals have opened up a new research field called topological semimetals [6]. Physically, the essence of topological band theory—that the Bloch wave function on a closed surface in momentum space can have nontrivial topological structures—is independent of the statistics of the constituent particles [7–9]. By replacing the electronic spin polarization in the above example by light polarization, for instance, one obtains a topological band crossing in photonic crystals. Such ideas of generalization have inspired researchers to find topologically nontrivial band crossings in boson systems of photons [10,11], phonons [12], and magnons in three [13] or lower dimensions [14–16].

Topological classification solely depends on symmetry class and dimensionality. There have been many studies on topological band crossings protected by lattice space-group symmetries [17–28], and an (almost) full classification of this type has appeared in the literature [29]. In this Letter, we focus on a new type of symmetry group: magnetic groups, which naturally rise in magnetically ordered systems. The difference between a magnetic group and a space group is that the former generically contains elements of the form ST , where S is a certain space-group operation and T time reversal [30], while neither S nor T is a symmetry. Band crossings protected by magnetic groups can be found in the electronic band structures in magnetic materials, as well as the band structure of magnons (coherent spin excitations) over a magnetic ground state.

We choose for our study one of the simplest magnetic groups, generated by PT , where P is spatial inversion. This magnetic group pertains to various antiferromagnets with centrosymmetric crystal lattices, where two spins related by

inversion have opposite polarizations in the ordered state. We first study the case where there is, in addition to PT , a global $U(1)$ spin-rotation symmetry seen in most collinear antiferromagnets—with or without an easy axis. We find that in the spin-wave dispersion the generic band crossings among the magnon branches are Dirac points having integer monopole charges. Furthermore, we find that when the $U(1)$ symmetry is broken [e.g., by Dzyaloshinsky-Moriya interactions (DMIs) [31,32] or other anisotropic effects], but PT still preserved, each Dirac point *necessarily* becomes a nodal line. Unlike all nodal lines thus far predicted for materials [33], this nodal line cannot continuously shrink to a point and disappear because it is protected by a new Z_2 monopole charge [34], aside from the π -Berry phase common to all nodal lines [34–38]. We apply the general theory to a three-dimensional “spin-web” compound, Cu_3TeO_6 [39,40], which develops a long-range and almost collinear antiferromagnetic order below $T_N \approx 61$ K. We use a J_1 - J_2 ($J_1 > J_2 > 0$) Heisenberg model to describe the spin interactions and calculate the magnon band structure using linear-spin-wave approximation, where multiple pairs of Dirac points are identified between two optical magnon branches. Then we add Dzyaloshinsky-Moriya interactions to the model and calculate the new classical ground state as well as the spin-wave excitations over the noncollinear ground state. Comparing this to the previous results, we find that each Dirac point now becomes a nodal line whose size is proportional to the strength of the DMIs squared. Experiments for detecting key features of Dirac and nodal line magnons are proposed.

General theory.—We begin by noting that when the total S_z is preserved [i.e., with $U(1)$ symmetry], all

single-particle excitations can be labeled by their spin quantum numbers. For magnons, these numbers are $+1$ and -1 , and magnons with opposite spins are decoupled in a quadratic Hamiltonian. Next we look at how the magnetic-group symmetry PT acts on the magnons. Physically, spatial inversion preserves spin and time reversal inverts it, making the composite symmetry PT invert the spin quantum number of a magnon. Based on these observations, we see that the single-particle Hamiltonian decouples into two sectors, one for each spin quantum number, or, symbolically,

$$H = H_+ \oplus H_-, \quad (1)$$

where H_{\pm} is the Hamiltonian for the spin- ± 1 sector in the spin system. The magnetic-group symmetry PT then requires

$$H_+ = H_-^*. \quad (2)$$

When H_+ is defined in the three-dimensional Brillouin zone, there can be Weyl points in the spectrum as band crossings [1]. Owing to Eq. (2), H_- and H_+ have the same band structure and, therefore, when a Weyl point appears in H_+ , there must be another Weyl point in H_- at the same (crystal) momentum. Since PT symmetry reverses the Berry curvature, these two Weyl points are of opposite monopole charge, so together they make a Dirac point. To follow are some basic properties of these Dirac points in the bulk. (i) The Weyl points in H_+ are not pinned to any high-symmetry point, line, or plane, so the Dirac point may appear at any momentum in the Brillouin zone, in contrast to previously studied Dirac points that are pinned to high-symmetry points and lines. (ii) Since the Weyl points in H_+ must appear in pairs, so also do the Dirac points in H . (iii) For each Dirac point, we can define a monopole charge as the monopole charge of the associated Weyl point in H_+ , a Z index.

In realistic magnetic materials, besides the isotropic Heisenberg terms, other terms, such as site-dependent single-ion anisotropy and exchange anisotropy, may break the $U(1)$ spin-rotation symmetry but will leave the space-time symmetry PT intact (or there would be ferroelectricity). For example, when the bonds connecting two magnetic atoms to their common ligand atom make an angle less than 180° , DMI is, in general, present. When $U(1)$ symmetry is broken, a Dirac point is no longer stable, and as long as PT is still preserved, Weyl points are disallowed [1], so, in principle, a Dirac point must be either fully gapped out or broken into a nodal line. Further analysis rules out the former possibility, and shows that each Dirac point becomes a nodal line upon turning on these anisotropic perturbations. To see this, we notice that as long as PT symmetry is preserved, even in the absence of $U(1)$ symmetry, a Z_2 -topological invariant can still be defined on a sphere surrounding the Dirac point, which is found to be nontrivial (see Ref. [41] for the calculation) for any sphere containing one Dirac point (or an odd number). According to Ref. [34], the nontrivial

invariant indicates that the Dirac point is but a limiting case of a nodal line, which cannot be gapped out as long as PT is preserved. To the best of our knowledge, while nodal lines without Z_2 monopole charge have been proposed in many fermionic and bosonic systems [33], nodal lines carrying a nontrivial Z_2 monopole charge have not yet been predicted for any real materials.

Dirac magnons in Cu_3TeO_6 .—Three-dimensional collinear antiferromagnets are the best platform for us to realize these topological band crossings in k space. Here, we have chosen Cu_3TeO_6 , which was reported to host a novel spin lattice [39], dubbed a three-dimensional spin web [40,46]. The lattice consists of almost coplanar Cu^{2+} hexagons that are perpendicular to one of the four space diagonals of the cubic unit cell (Fig. 1), featuring a hybrid between a 3D spin-1/2 network and a low connectivity of interactions between neighbors: each Cu^{2+} ion is shared by two hexagons and has only four nearest neighbors (and four next-nearest neighbors). Below $T_N \approx 61$ K, the system develops long-range antiferromagnetic order that leaves clear signatures in magnetic susceptibility and neutron diffraction measurements [39]. Without loss of generality, we believe that the large yet highly symmetric magnetic primitive cell of Cu_3TeO_6 is favorable for symmetry-protected magnon band crossings.

Furthermore, we note that the lattice structure of Cu_3TeO_6 is very similar to those of C -type sesquioxides $R_2\text{O}_3$ ($R = \text{Y}, \text{Sc}, \text{In}$, or a rare-earth element) [47]. The spin lattice of Cu_3TeO_6 can be realized in the latter if the Wyckoff $24d$ and $8a$ sites could be occupied, respectively, by magnetic or nonmagnetic ions. Given the rather broad distribution of the R^{3+} ionic radii, ranging from 81 pm (Sc and In) to 106 pm (La), it might be possible to synthesize solid solutions of them, such as Nd_3ScO_6 , with minimal intersite disorder [48]. Along with the rich magnetic properties of rare-earth elements, this renders our analysis

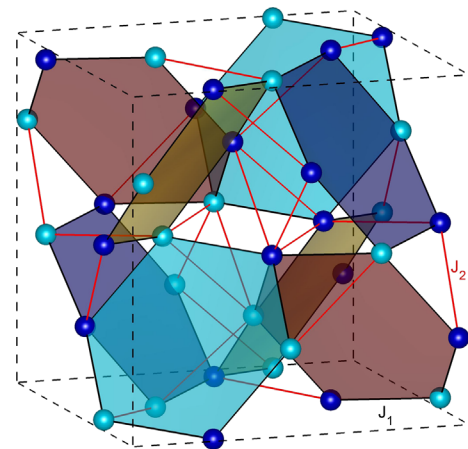


FIG. 1. The Cu^{2+} sublattice of Cu_3TeO_6 in a cubic unit cell, with spin-up and -down ions represented by different colors. Nearest-neighbor (J_1) and next-nearest-neighbor (J_2) interactions are indicated.

of Cu_3TeO_6 potentially applicable to a large family of interesting magnetic materials.

Available neutron diffraction data are consistent with a collinear antiferromagnetic spin configuration depicted in Fig. 1, although a slightly noncollinear tilting cannot be ruled out [39]. In this section, we assume the collinear ground state, i.e., $U(1)$ spin-rotation symmetry, and in the next we include Dzyaloshinsky-Moriya interactions to account for the effect of noncollinearity. The collinear ground state is most easily understood by assuming the unfrustrated nearest-neighbor Heisenberg exchange interaction $J\mathbf{S}_i \cdot \mathbf{S}_j$. Yet, because of the geometric configuration of the atoms, the next-nearest-neighbor exchange may also have an appreciable magnitude whose sign is also likely to be positive (antiferromagnetic). We thus model the spin interactions in Cu_3TeO_6 using the following J_1 - J_2 Heisenberg model:

$$H = J_1 \sum_{\langle ij \rangle} \mathbf{S}_i \cdot \mathbf{S}_j + J_2 \sum_{\langle\langle ij \rangle\rangle} \mathbf{S}_i \cdot \mathbf{S}_j. \quad (3)$$

The classical ground state of H depends on the relative magnitude of J_1 and J_2 , and when $J_2 < J_c = J_1/3$, the ground state configuration matches the experimental one shown in Fig. 1. It is easy to verify that this spin configuration preserves both PT and S_z , and hence it may host Dirac magnons. Assuming strongly localized moments and negligible quantum fluctuations, we treat the magnon excitations using the linear spin-wave approximation. There are 12 spins in each primitive cell, with six pointing positive (along a domain-dependent $\langle 111 \rangle$ -direction [39], which we refer to as the $[111]$ -direction) and six negative in the ground state. (Note that the magnetic order does not enlarge the lattice primitive cell.) We perform the standard Holstein-Primakoff transformation on the up spins,

$$S_+ = \sqrt{2S}a, \quad S_z = S - a^\dagger a, \quad (4)$$

and down spins,

$$S_+ = -\sqrt{2S}b^\dagger, \quad S_z = -S + b^\dagger b, \quad (5)$$

where $S_\pm \equiv S_x \pm iS_y$. We remark that, under spin rotation along the z axis through θ , spin-wave operator a transforms as $a \rightarrow ae^{-i\theta}$ on up spins and $b \rightarrow be^{i\theta}$ on down spins, making them $S_z = +1$ and -1 operators, respectively. All spin-wave operators can thus be divided into two sets by their spins: $\{a, b^\dagger\}$ having $S_z = +1$ and $\{a^\dagger, b\}$ having $S_z = -1$. As long as the $U(1)$ symmetry is present, these two sets do not couple to each other in a quadratic spin-wave Hamiltonian. The steps we take to find and solve the spin-wave Hamiltonian are given in Ref. [41].

For $J_2 = 0.134J_1$ (see Ref. [41] for other values of J_2), the magnon bands along high-symmetry lines in the Brillouin zone are plotted in Fig. 2(a). Distinct linear band crossings can be found between the two optical branches in pale yellow. Calculation of the monopole charge using the Wilson loop technique confirms that all of these band

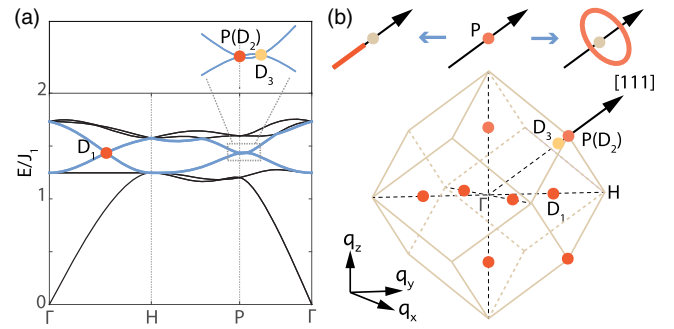


FIG. 2. (a) A typical band structure of the spin-wave dispersion along high-symmetry lines with $J_2 = 0.134J_1 > 0$, where the inset shows an enlarged region near P . (b) Positions of all Dirac points in the first Brillouin zone. Red and yellow indicate, respectively, a monopole charge of $+1$ or -1 . For clarity, only one of the eight D_3 points is displayed in the three-dimensional Brillouin zone in (b). Above the Brillouin zone, we schematically show how, upon adding the DMIs, a Dirac point at P expands either into a nodal ring around $[111]$ or into a line along $[111]$, preserving the threefold rotation along the $[111]$ axis.

crossings are Dirac points (or Weyl points in H_+): there are six positive Dirac points along ΓH and its symmetry equivalents (denoted by D_1), two positive Dirac points at two P points (D_2), and eight negative Dirac points along ΓP and its symmetry equivalents (D_3). More detailed search shows that there is no other band crossing between these two branches.

We remark that the limited experimental data in the literature on this compound cannot fully justify the J_1 - J_2 model (or any spin model), so that the positions of $D_{1,3}$ and even their appearance depend on specifics of the model. Nonetheless, we emphasize that the high-symmetry point P (D_2) is *always* a Dirac point. This *model independent* Dirac point deserves the detailed analysis given below. The three screw rotations $R_{x,y,z}$ and PT are elements of the little group at P . It is straightforward to verify that

$$\{R_i, R_j\} = -2\delta_{ij}. \quad (6)$$

iR_i matrices are hence generators of a Clifford algebra, the simplest choice of which are the Pauli matrices, i.e., $R_i = i\sigma_i$. Since both space inversion and time reversal commute with R_i , PT commutes with R_i , so R_i must be real. However, since $i\sigma_{x,z}$ are imaginary, PT excludes this simplest choice. The next choice is that R_i are Dirac matrices, and out of the five generators one can pick $R_x = i\sigma_y s_x$, $R_y = i\sigma_y$, and $R_z = \pm i\sigma_y s_z$, which are real and satisfy Eq. (6). This proof shows that all levels at point P are at least fourfold degenerate. When $U(1)$ symmetry is present, the two P points in the BZ are found to have the same monopole charge of either $+1$ or -1 .

Topological nodal lines in Cu_3TeO_6 .—Owing to the less than 180° bond angle of the Cu-O-Cu bond, the DMI generally exists between nearest-neighbor spins:

$$H_{\text{DM}} = \sum_{\langle ij \rangle} D \hat{\mathbf{d}}_{ij} \cdot \mathbf{S}_i \times \mathbf{S}_j, \quad (7)$$

where D is the magnitude and $\hat{\mathbf{d}}_{ij}$ is the normal direction of the triangle made from the three atoms in the Cu—O—Cu bond.

The collinear ground state is unstable upon turning on the interaction, but when D is small, there are stable configurations close to the collinear one with spins pointing along the [111] direction. In Figs. 3(a) and 3(b), we show the classical ground state configuration for $D/J_1 = 0.2$ (calculated from a quasi-Newton method), and the directions of all spins are given in polar coordinates in the table in Fig. 3(c). This result is fully consistent with the neutron diffraction results [39] and, in the limit in which D is infinitesimally small, it provides a natural explanation for the (collinear) ground state spin orientation along the [111] direction, which cannot be explained by the Heisenberg model.

While the noncollinear ground state breaks many symmetries of the lattice, such as the three screw axes, it preserves PT and threefold rotation along the [111] direction. To calculate the spin-wave excitations above the noncollinear ground state, one need only notice that the spin components in the absolute frame of reference and those in the frame of reference on each site are related by a site-dependent rotation matrix R_i . The spin-wave Hamiltonian becomes

$$H' = J_1 \sum_{\langle ij \rangle} R_i \mathbf{S}_i \cdot R_j \mathbf{S}_j + J_2 \sum_{\langle\langle ij \rangle\rangle} R_i \mathbf{S}_i \cdot R_j \mathbf{S}_j + D \sum_{\langle ij \rangle} \hat{\mathbf{d}}_{ij} \cdot R_i \mathbf{S}_i \times R_j \mathbf{S}_j, \quad (8)$$

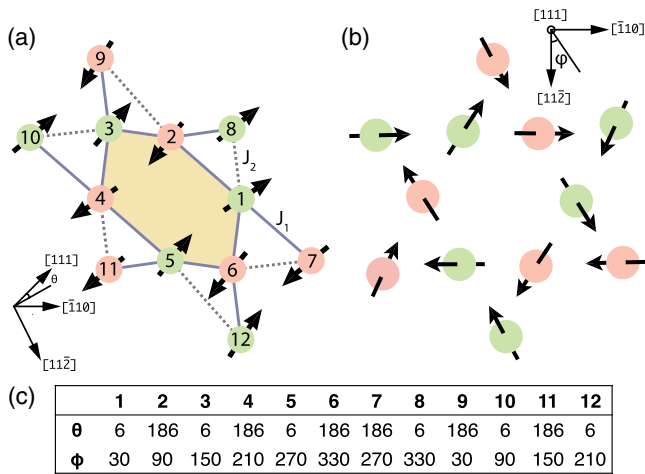


FIG. 3. (a) The classical ground state configuration for $D/J_1 = 0.2$. Spin-up and -down ions are represented by different colors with nearest-neighbor (J_1) and next-nearest-neighbor (J_2) interactions indicated. (b) The same configuration projected on the (111) plane. (c) Table of the exact direction of each polarization, where angle θ and ϕ are defined in the corner panels of (a),(b).

where the components in \mathbf{S}_i are given in Eqs. (4) and (5). Since both the spin interactions and the noncollinear ground state configuration preserve PT and C_3 , H' also has these symmetries. The experimental tilting angle is small, implying that DMI may be considered as a perturbation to the original Hamiltonian in Eq. (3). In this case, we can expand R_i in powers of D and collect all terms up to D^2 into $\delta H \equiv H' - H$. To gain an understanding of how DMI affects the Dirac points, we project δH onto the subspace spanned by the four degenerate states at P , finding a $k \cdot p$ effective Hamiltonian for the spin waves near P . Because of the C_3 symmetry, we expect a Dirac point at P to either break into a ring around the [111] direction or extend into a straight line along [111], which may be considered the limiting case of an eclipse with a vanishing short axis [see the upper panel of Fig. 2(b) for schematics of the two scenarios]. In Ref. [41], we show that either scenario may occur, depending on which four degenerate states at P are considered: (i) the Dirac point between the first and the second band (both degenerate) at P becomes a nodal ring, and (ii) the Dirac point between the third and the fourth band is stretched into a straight line. In both cases, however, the length of the nodal line is found to be proportional to D^2 , and the center of the nodal line is displaced from P by a distance proportional to D . Here, we only picked Dirac points at P for this analysis; this is because they are the only Dirac points whose existence and position are independent of specifics of the Heisenberg model, and hence they are most likely to be observed in experiments.

Discussion.—Finally, we remark on possible experiments that will be able to justify our assumptions and testify to our predictions. The Dirac points as well as nodal rings in the bulk can be directly measured with inelastic neutron scattering, and they are further expected to exhibit gap-opening behaviors in a magnetic field. Since magnons of each spin form many Weyl points, there are thermal Hall currents for each spin component. However, because the total Hall current of magnons must vanish due to PT , a spin-resolved measurement of the magnon currents is required to observe this effect. The surface arc states, however interesting (see Ref. [41] for a detailed calculation), are difficult to directly observe by inelastic neutron scattering due to the very small sample volume from the surfaces. One may be able to detect these states using surface-sensitive probes, such as high-resolution electron energy loss spectroscopy, or helium atom energy loss spectroscopy.

We wish to thank Ji Feng, Fa Wang, Xuetao Zhu, Ling Lu, and R. Ganesh for the discussions and Weiliang Yao for the assistance in checking some of our early calculations. The work at the Institute of Physics was supported by the National Key Research and Development Program of China under Grant No. 2016YFA0302400, by NSFC under Grants No. 11674370, No. 1190020, No. 11534014, and No. 11334012, by the Ministry of Science and Technology of China 973 program (Grant No. 2015CB921300), and by

the Strategic Priority Research Program of CAS (Grant No. XDB07000000). The work at Peking University was supported by the National Natural Science Foundation of China (Grants No. 11374024 and No. 11522429) and the Ministry of Science and Technology of China (Grants No. 2015CB921302 and No. 2013CB921903).

K. L. and C. L. contributed equally to this work.

* yuan.li@pku.edu.cn

† cfang@iphy.ac.cn

- [1] S. Murakami, *New J. Phys.* **9**, 356 (2007).
- [2] X. Wan, A. M. Turner, A. Vishwanath, and S. Y. Savrasov, *Phys. Rev. B* **83**, 205101 (2011).
- [3] B. Q. Lv, H. M. Weng, B. B. Fu, X. P. Wang, H. Miao, J. Ma, P. Richard, X. C. Huang, L. X. Zhao, G. F. Chen, Z. Fang, X. Dai, T. Qian, and H. Ding, *Phys. Rev. X* **5**, 031013 (2015).
- [4] S.-Y. Xu, I. Belopolski, N. Alidoust, M. Neupane, C. Zhang, R. Sankar, S.-M. Huang, C.-C. Lee, G. Chang, B. Wang, G. Bian, H. Zheng, D. S. Sanchez, F. Chou, H. Lin, S. Jia, and M. Z. Hasan, *Science* **349**, 613 (2015).
- [5] L. Lu, Z. Wang, D. Ye, L. Ran, L. Fu, J. D. Joannopoulos, and M. Soljacic, *Science* **349**, 622 (2015).
- [6] A. A. Burkov, *Nat. Mater.* **15**, 1145 (2016).
- [7] F. D. M. Haldane and S. Raghu, *Phys. Rev. Lett.* **100**, 013904 (2008).
- [8] L. Lu, J. D. Joannopoulos, and M. Soljacic, *Nat. Photonics* **8**, 821 (2014).
- [9] S. D. Huber, *Nat. Phys.* **12**, 621 (2016).
- [10] L. Lu, L. Fu, J. D. Joannopoulos, and M. Soljacic, *Nat. Photonics* **7**, 294 (2013).
- [11] L. Wang, S.-K. Jian, and H. Yao, *Phys. Rev. A* **93**, 061801 (2016).
- [12] O. Stenull, C. L. Kane, and T. C. Lubensky, *Phys. Rev. Lett.* **117**, 068001 (2016).
- [13] F.-Y. Li, Y.-D. Li, Y. B. Kim, L. Balents, Y. Yu, and G. Chen, *Nat. Commun.* **7**, 12691 (2016).
- [14] J. Fransson, A. M. Black-Schaffer, and A. V. Balatsky, *Phys. Rev. B* **94**, 075401 (2016).
- [15] S. A. Owerre, *J. Phys. Condens. Matter* **28**, 386001 (2016).
- [16] S. A. Owerre, *J. Phys. Commun.* **1**, 025007 (2017).
- [17] S. M. Young, S. Zaheer, J. C. Y. Teo, C. L. Kane, E. J. Mele, and A. M. Rappe, *Phys. Rev. Lett.* **108**, 140405 (2012).
- [18] Z. Wang, Y. Sun, X.-Q. Chen, C. Franchini, G. Xu, H. Weng, X. Dai, and Z. Fang, *Phys. Rev. B* **85**, 195320 (2012).
- [19] Z. Wang, H. Weng, Q. Wu, X. Dai, and Z. Fang, *Phys. Rev. B* **88**, 125427 (2013).
- [20] B.-J. Yang and N. Nagaosa, *Nat. Commun.* **5**, 4898 (2014).
- [21] C. Fang, L. Lu, J. Liu, and L. Fu, *Nat. Phys.* **12**, 936 (2016).
- [22] B. Bradlyn, J. Cano, Z. Wang, M. G. Vergniory, C. Felser, R. J. Cava, and B. A. Bernevig, *Science* **353**, aaf5037 (2016).
- [23] H. Weng, C. Fang, Z. Fang, and X. Dai, *Phys. Rev. B* **93**, 241202 (2016).
- [24] Z. Zhu, G. W. Winkler, Q. S. Wu, J. Li, and A. A. Soluyanov, *Phys. Rev. X* **6**, 031003 (2016).
- [25] G. Chang, S.-Y. Xu, S.-M. Huang, D. S. Sanchez, C.-H. Hsu, G. Bian, Z.-M. Yu, I. Belopolski, N. Alidoust, H. Zheng, T.-R. Chang, H.-T. Jeng, S. A. Yang, T. Neupert, H. Lin, and M. Z. Hasan, *Sci. Rep.* **7**, 1688 (2017).
- [26] B. J. Wieder, Y. Kim, A. M. Rappe, and C. L. Kane, *Phys. Rev. Lett.* **116**, 186402 (2016).
- [27] B.-J. Yang, T. A. Bojesen, T. Morimoto, and A. Furusaki, *Phys. Rev. B* **95**, 075135 (2017).
- [28] S. M. Young and B. J. Wieder, *Phys. Rev. Lett.* **118**, 186401 (2017).
- [29] H. Watanabe, H. C. Po, M. P. Zaletel, and A. Vishwanath, *Phys. Rev. Lett.* **117**, 096404 (2016).
- [30] C. J. Bradley and B. L. Davies, *Rev. Mod. Phys.* **40**, 359 (1968).
- [31] I. Dzyaloshinsky, *J. Phys. Chem. Solids* **4**, 241 (1958).
- [32] T. Moriya, *Phys. Rev.* **120**, 91 (1960).
- [33] C. Fang, H. Weng, X. Dai, and Z. Fang, *Chin. Phys. B* **25**, 117106 (2016).
- [34] C. Fang, Y. Chen, H.-Y. Kee, and L. Fu, *Phys. Rev. B* **92**, 081201 (2015).
- [35] A. A. Burkov, M. D. Hook, and L. Balents, *Phys. Rev. B* **84**, 235126 (2011).
- [36] G. Xu, H. Weng, Z. Wang, X. Dai, and Z. Fang, *Phys. Rev. Lett.* **107**, 186806 (2011).
- [37] G. E. Volovik, *J. Supercond. Novel Magn.* **26**, 2887 (2013).
- [38] Y. Kim, B. J. Wieder, C. L. Kane, and A. M. Rappe, *Phys. Rev. Lett.* **115**, 036806 (2015).
- [39] M. Herak, H. Berger, M. Prester, M. Miljak, I. Živković, O. Milat, D. Drobac, S. Popović, and O. Zaharko, *J. Phys. Condens. Matter* **17**, 7667 (2005).
- [40] K. Y. Choi, P. Lemmens, E. S. Choi, and H. Berger, *J. Phys. Condens. Matter* **20**, 505214 (2008).
- [41] See Supplemental Material at <http://link.aps.org/supplemental/10.1103/PhysRevLett.119.247202>, which includes Refs. [42–45], for further details on the derivation of spin-wave Hamiltonian, magnon band structures at other parameters, Z_2 -monopole charge of the Dirac point, and the surface arc states in Cu_3TeO_6 .
- [42] P. Villars and K. Cenzual, *Pearson's Crystal Data: Crystal Structure Database for Inorganic Compounds, Release 2017/18 (on CD)* (ASM International, Materials Park, OH, 2017).
- [43] S.-Y. Xu, C. Liu, S. K. Kushwaha, R. Sankar, J. W. Krizan, I. Belopolski, M. Neupane, G. Bian, N. Alidoust, T.-R. Chang *et al.*, *Science* **347**, 294 (2015).
- [44] M. P. L. Sancho, J. M. L. Sancho, and J. Rubio, *J. Phys. F* **14**, 1205 (1984).
- [45] M. P. L. Sancho, J. M. L. Sancho, and J. Rubio, *J. Phys. F* **15**, 851 (1985).
- [46] M. Mansson, K. Prsa, J. Sugiyama, D. Andreica, H. Luetkens, and H. Berger, *Phys. Procedia* **30**, 142 (2012).
- [47] E. N. Maslen, V. A. Streltsov, and N. Ishizawa, *Acta Crystallogr. Sect. B* **52**, 414 (1996).
- [48] B. Antic, M. Mitric, and D. Rodic, *J. Magn. Magn. Mater.* **145**, 349 (1995).